



Electromagnetics

ISSN: (Print) (Online) Journal homepage: www.tandfonline.com/journals/uemg20

Quad-PortMIMO dielectric ResonatorAntenna with filtering response for IoT application

Abhimanyu Yadav, Deepak Sigroha, Manish Tiwari & Anand Sharma

To cite this article: Abhimanyu Yadav, Deepak Sigroha, Manish Tiwari & Anand Sharma (2024) Quad-PortMIMO dielectric ResonatorAntenna with filtering response for IoT application, *Electromagnetics*, 44:1, 32-45, DOI: [10.1080/02726343.2024.2305925](https://doi.org/10.1080/02726343.2024.2305925)

To link to this article: <https://doi.org/10.1080/02726343.2024.2305925>



Published online: 18 Jan 2024.



Submit your article to this journal 



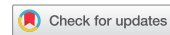
Article views: 77



View related articles 



View Crossmark data 



Quad-PortMIMO dielectric ResonatorAntenna with filtering response for IoT application

Abhimanyu Yadav^a, Deepak Sigroha^b, Manish Tiwari^a, and Anand Sharma^a 

^aDepartment of Electronics and Communication Engineering, Motilal Nehru National Institute of Technology Allahabad, Prayagraj, India; ^bDepartment of Electronics Engineering, Rajkiya Engineering College, Sonbhadra, India

ABSTRACT

This article presents a four-port Multi-Input Multi-Output (MIMO) antenna based on Dielectric Resonators (DR), showcasing excellent filtering characteristics, high isolation between ports, and strong diversity performance. The initial step introduces a single-port filtering Dielectric Resonator Antenna (DRA) utilizing the HEM₁₁₆ mode, featuring a complementary split ring resonator (SRR) feed structure that excites the cylindrical DR. This feed structure enables the independent adjustment of one resonance frequency and two radiation nulls. The experimental results confirm that the designed radiator works in between 2.35 and 2.57 GHz with an isolation level of more than 25 dB. The value of the gain is around 5.0 dBi within the operating band, while it is less than -15 dBi outside the working band. All these features make the designed MIMO radiator applicable for IoT applications.

ARTICLE HISTORY

Received 10 November 2023
Revised 03 January 2024
Accepted 9 January 2024

KEYWORDS

Dielectric resonator antenna;
MIMO; mutual coupling

Introduction

In the modern landscape of wireless communication, the prominence of dielectric resonator-based MIMO antennas is notable, primarily attributed to two crucial factors: firstly, their capacity to attain a high Signal-to-Noise Ratio (SNR) without requiring adjustments in transmission power (Sharawi 2014); and secondly, their proficiency in enabling effective multi-channel communication within a condensed form factor (Petosa 2007). In the pursuit of achieving a more streamlined wireless communication system, the design of filtering antennas has gained significant popularity within the academic literature. The incorporation of a filtenna obviates the need for a separate bandpass filter at the output of the antenna, simplifying system architecture and enhancing overall efficiency (Dhwaj et al. 2018). In the literature, distinct researchers have individually addressed antenna design with filtering responses, utilizing two primary methods: the filter synthesis approach (Yusuf, Cheng, and Gong 2011)- (Mao et al. 2016) and the antenna fusion approach (Hu et al. 2018)- (Yadav, Tiwari, and Sharma 2023). In the first technique, the filter is initially realized, followed by the implementation of the radiator at the end of the filtering structure. On the contrary, the latter approach emphasizes antenna design, achieving the filtering function by incorporating basic parasitic elements like slots (Jin, Liao, and Xue 2018), coupled strips (Hu et al. 2016), or shorting vias (Hu et al. 2017) to manipulate the antenna's input impedance. In general, while

both methods yield comparable filtering performance, the fusion design approach offers more compact structures and enhanced radiation performance due to the absence of filtering circuits and associated insertion loss, leading to higher antenna gain and efficiency. In a recent study, researchers utilized a microstrip coupled slot configuration as the feeding mechanism for Dielectric Resonator Antennas (DRAs). They integrated parasitic strips (Hu et al. 2016) or shorting vias (Hu et al. 2017) into the feeding microstrip line. This innovative approach allowed them to strategically introduce radiation nulls within the stopband, thereby achieving effective filtering functionality within the antenna system. In (Pan et al. 2018), dual stubs along with a conformal strip are utilized to feed the rectangular shaped ceramic for creating radiation nulls at 1.6 GHz and 2.3 GHz (outside the operating band). In (Yadav, Tiwari, and Sharma 2023), dual cylindrical ceramic fed using circular patch to create radiation nulls outside the working band for producing filtering features. In (Liu, Leung, and Yang 2021), a Dielectric Resonator Antenna (DRA) utilizes a feed structure consisting of three slots of varying lengths. This configuration results in the creation of two radiation nulls positioned near the passband's edges. Additionally, in (Wang et al. 2021), a combination of a slot line with stepped-impedance resonator characteristics and the transverse arm of a microstrip feedline enables the generation of three radiation nulls.

This article presents a four-port MIMO antenna based on Dielectric Resonators (DR), which works between 2.35 and 2.57 GHz. Orthogonal orientation of ports provides a good isolation level among the ports, i.e. more than 25 dB. Rectangular complementary split ring resonator (RCSRR) is utilized to create the radiation nulls at 2.29 GHz and 2.69 GHz, respectively. This feed structure enables the independent adjustment of one resonance frequency and two radiation nulls. The proposed article is divided into different sections: (1) analysis of single-port filtering DRA; (2) analysis of four-port filtering DRA; (3) experimental result; (4) conclusion; and (5) reference.

Analysis of single port filtering DRA

Configuration

As shown in [Figure 1](#), the proposed filtering Dielectric Resonator Antenna (DRA) consists of a cylindrical DR with a dielectric constant of 9.8. This is paired with a substrate that has a relative dielectric constant of 4.4 and a thickness of 0.8 mm. On the upper part of the substrate, there is a feed structure, which includes both a driven modified rectangular strip and a parasitic modified rectangular strip (which looks like a complementary split ring resonator). Notably, a conformal strip is used at the edge of the dielectric to feed it properly. [Table 1](#) gives the dimension of the different parameters of single-port filtenna.

Antenna mechanism

[Figure 2](#) illustrates the evolutionary steps of the proposed filtering Dielectric Resonator Antenna's working mechanism, with a change in the feed structures of DRA. From [Figure 2](#), it can be seen that antenna-1 is simply DRA stimulated by a driven modified rectangle. Antenna-2 is obtained by adding the parasitic rectangular element to the driven element. In

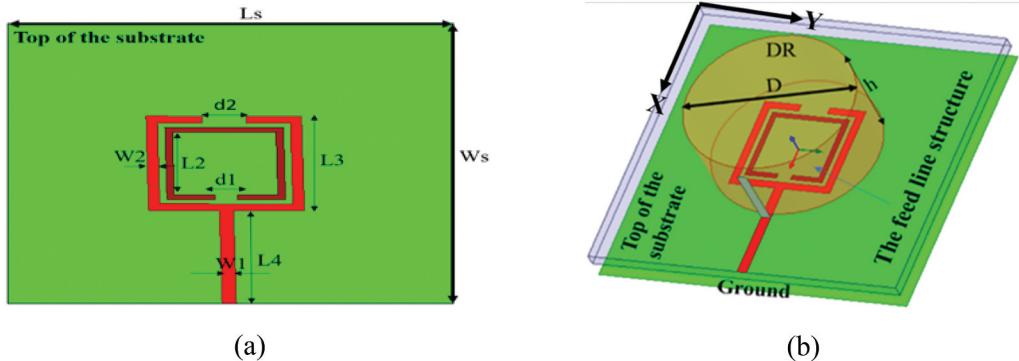


Figure 1. Configuration of proposed Single-port CDRA(a) top view of feed structure (b)3D-view of proposed filtering CDRA.

Table 1. Optimized dimension of various parameters of single-port filtnenna.

Parameter	Dimension (mm)	Parameter	Dimension (mm)
Ws	60.0	W2	2.0
Ls	60.0	D	25.0
W1	2.0	h	12.0
L1	10.0	L2	7.0
L3	10.0	L4	12.0
d1	3.3	d2	6.3

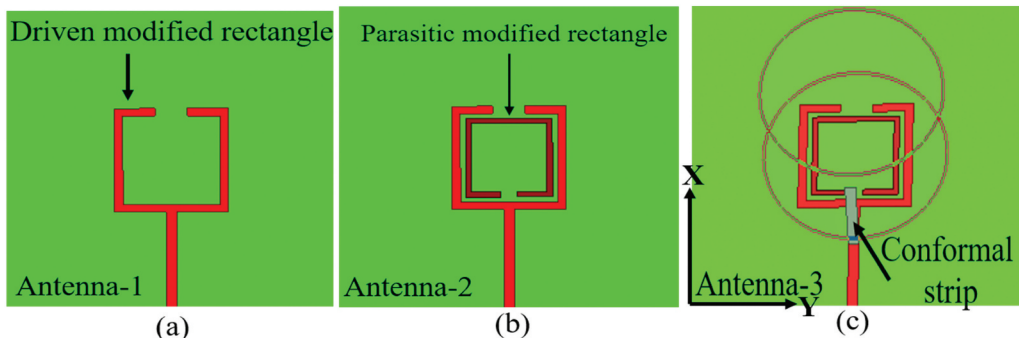


Figure 2. Evolution diagram of CDRA feed structure (a) antenna-1 (b) antenna-2 (c) antenna-3.

Antenna-3, a conformal strip is added to the edge of the cylindrical dielectric along with driven and parasitic elements. Figure 3(a, b) represent the $|S_{11}|$ parameter and realized gain for evolutionary steps.

Two observations can be perceived from Figure 3(a): (i) impedance matching is very poor for the resonant peak at 2.39 GHz for antenna-1 and antenna-2; (ii) addition of conformal strip improves the impedance matching of the proposed single-port DRA. This is because there is a requirement of a vertical current source to feed the low dielectric constant ceramic (Petosa 2007). Similarly, it is observed

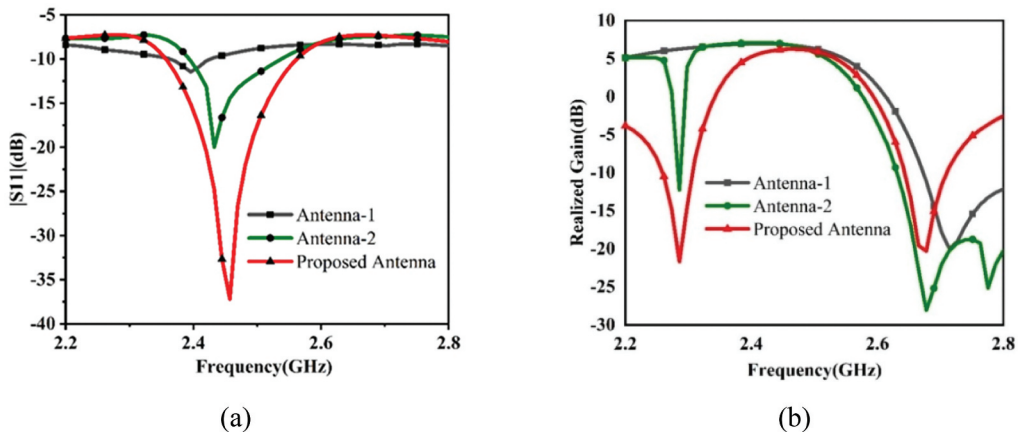


Figure 3. Different modifications in feeding structures of designed single port radiator (a) reflection coefficient ($|S_{11}|$) (b) realized gain.

from Figure 3(b) that a single-driven modified rectangular strip is accountable for the radiation null at 2.75 GHz (upper radiation null). The parasitic modified rectangular strip along with the driven rectangular strip is accountable for radiation null at 2.28 GHz. The addition of a conformal strip enhances the roll-off factor of the proposed filtering Dielectric Resonator Antenna (DRA).

Mode analysis of proposed Antenna

The resonant mode analysis of the proposed filtering Dielectric Resonator Antenna (DRA) entails a comprehensive examination of internal electric field distributions, as depicted in Figure 4. It is noteworthy that the electric field distributions exhibit a substantial degree of uniformity within the XY-plane, while discernible disparities emerge within the YZ-plane (none of them can reach one-half wavelength). Hence, it can be concluded that $HEM_{11\delta}$ mode is created inside the cylindrical ceramic. According to (Martin et al. 0000), the resonant frequency of the $HEM_{11\delta}$ mode can be roughly calculated through

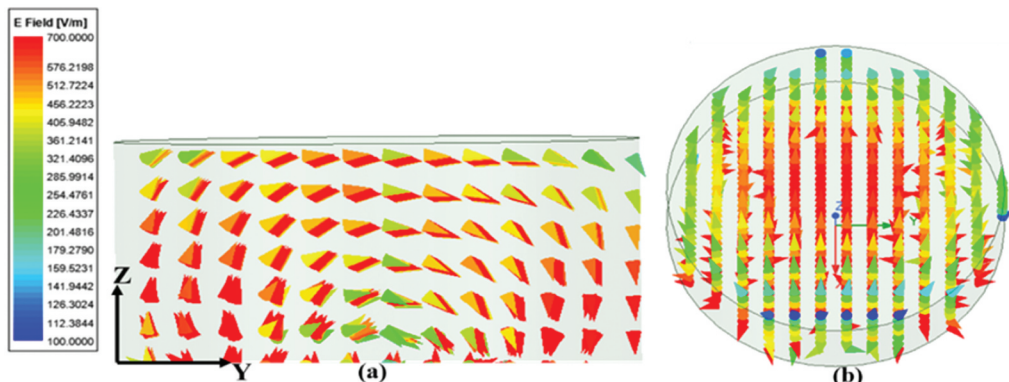


Figure 4. Electric-field distribution inside CDR at 2.45 GHz (a) side view (b) top view.

$$f_{r, \text{HEM}_{11\delta}} = \frac{6.324 * C}{2\pi D \sqrt{\epsilon_{\text{Alumina}}}} \left\{ 0.27 + 0.36 \left(\frac{D}{2h} \right) + 0.02 \left(\frac{D}{2h} \right)^2 \right\} \quad (1)$$

In the aforementioned equation, “c” represents the propagation velocity of light in free space, “ ϵ ” stands for the dielectric constant of the cylindrical Dielectric Resonator (DR), while “r” and “h” correspond to the radius and height of the cylindrical DR, respectively. Our calculations have yielded a resonant frequency of approximately 2.45 GHz for $\text{HEM}_{11\delta}$ mode, a result that closely aligns with our simulation data. This further substantiates the assertion that the resonant mode induced in this study unequivocally corresponds to the $\text{HEM}_{11\delta}$ mode.

Analysis of radiation nulls

The illustration above demonstrates that the proposed feeding structure serves a dual purpose: it not only generates supplementary DR resonances to augment the impedance bandwidth within the pass band but also facilitates the creation of radiation nulls, enabling the implementation of a filtering function. To delve into the generation mechanism of the radiation nulls, it becomes necessary to examine the electric field patterns within the DR of the antenna at 2.28 GHz and 2.68 GHz, which is shown in [Figure 5](#).

The electric fields excited by the conformal strip and those generated by the driven and parasitic-modified rectangle elements exhibit a notable similarity in magnitude but are distinctly out of phase with each other at both 2.28 GHz and 2.68 GHz. This phase discrepancy results in the production of radiation nulls, as the radiation emanating from the out-of-phase fields undergoes a near-complete cancellation effect.

Radiation nulls are controlled by variation in the parameter “d1” and “d2,” which is shown in [Figure 1\(a\)](#). To validate this observation, [Figure 6](#) illustrates the reflection coefficient and realized gain across various values of “d2.” Notably, it becomes evident that as “d2” increases, both the initial resonance within the pass band and the radiation null at the higher band edge exhibit an upward shift. Meanwhile, the response within the lower stopband remains relatively stable and undergoes little change. The investigation results for different lengths (d1) of the parasitic modified rectangle are presented in [Figure 7](#). In this scenario, it is evident that the response within the upper stopband remains largely unaffected by the variations in d1. However, there is a significant change in the lower band, with the radiation null shifting from 2.23 to 2.32 GHz. These findings suggest that it is

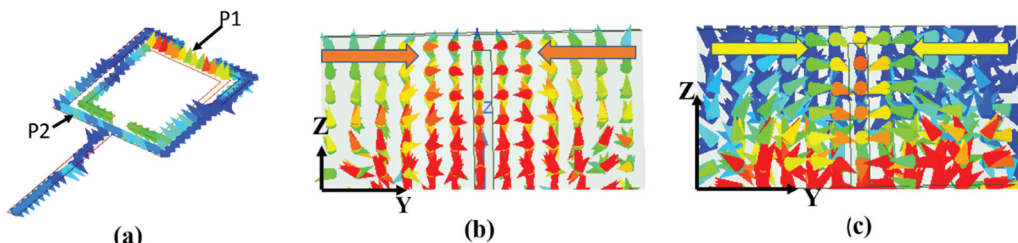


Figure 5. Simulated E-Field distribution (a)E-field at feed line at 2.28 GHz (b) radiation null at 2.68 GHz. (d) Radiation null at 2.28 GHz.

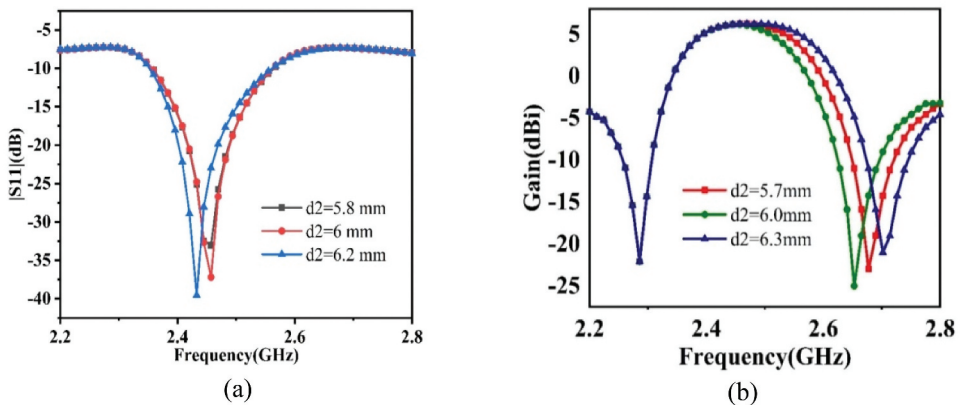


Figure 6. Effect of variation in 'd2' (a) $|S_{11}|$ (b) realized gain.

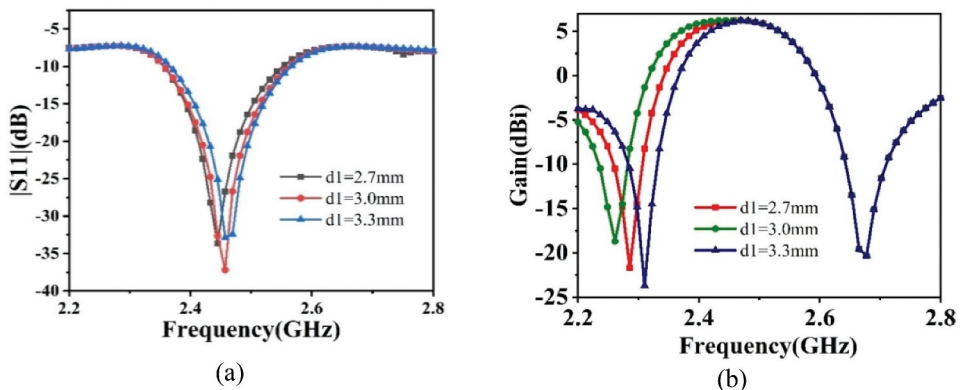


Figure 7. Effect of variation in 'd1' (a) $|S_{11}|$ (b) realized gain.

possible to independently tune the nulls by adjusting the values of d_1 and d_2 . This characteristic is highly desirable when designing filtering antennas. Figure 8 illustrates the impact of the gap between the driven and parasitic rectangles. From the observation of Figure 8, it is evident that an increase in the gap between the two rectangles leads to a corresponding shift to the right in both the response S_{11} and the gain.

Four-port filtering DRA

Configuration

This sub-section includes the proposed four-port CDRA, which is extended from single-port CDRA.

As shown in Figure 9, the proposed four-port filtering CDRA consists of a four-cylindrical DR with a dielectric constant of 9.8. The length and width of the substrate are found to be 100.0 mm and 100.0 mm respectively. Port-1 and port-2 are orthogonal to each

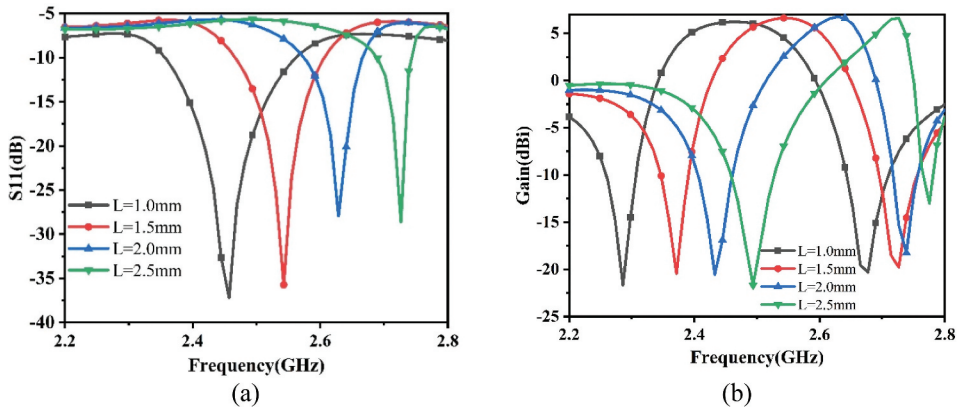


Figure 8. Effect of variation in L (gap in between driven and parasitic rectangle) (a) $|S_{11}|$ (b) realized gain.

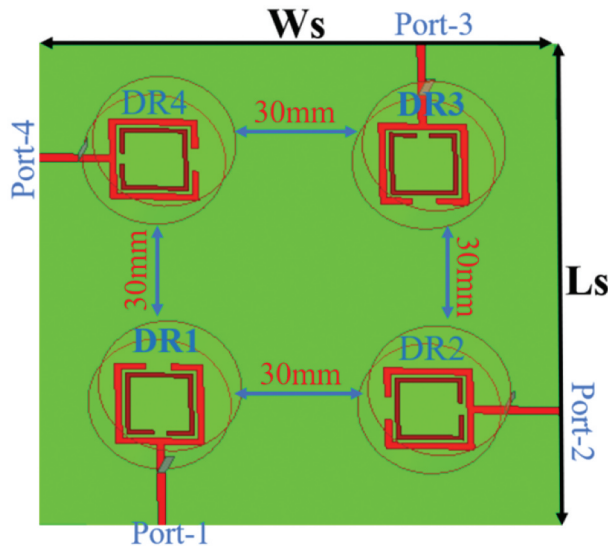


Figure 9. Configuration of proposed four-port CDRA.

other, while port-3 and port-4 are orthogonal. Similarly, port-1 positions orthogonally with port-4, and port-2 positions orthogonally with port-4. Figure 10 shows a different view of the prototype of the proposed radiator.

Analysis of four-port filtering antenna

Figure 11(a, b) show the S-parameter and gain variation of the proposed four-port MIMO antenna. From Figure 11(a), it is observed that the reflection coefficient is approximately the same as for a single port. The mutual coupling between the antenna ports is less than -25 dB. This is due to the combined effect of polarization diversity and space diversity. From Figure 11(b), it is confirmed that the gain pattern for single-port antenna and MIMO antenna is approximately the same.

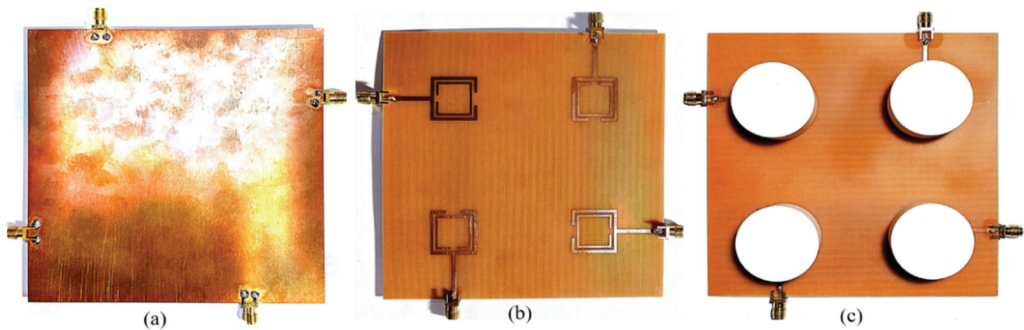


Figure 10. Proposed prototype of four-port MIMO (a)Bottom view (b)Feeding structure (c)3D view of the proposed radiator.

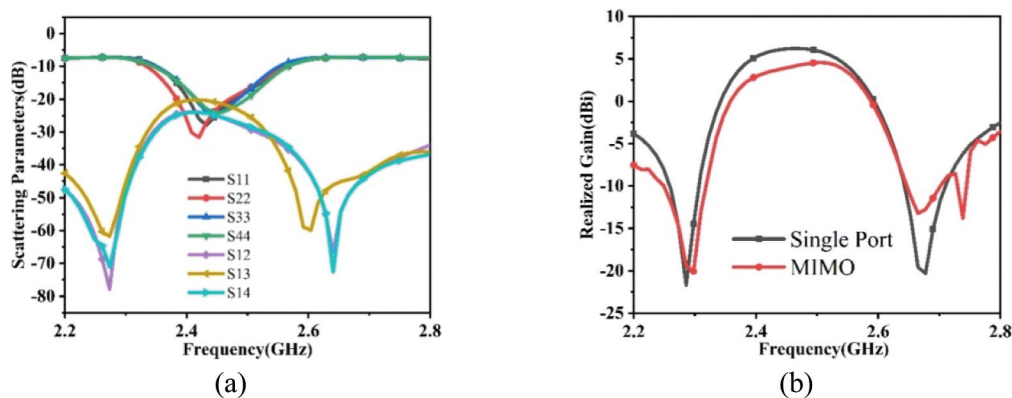


Figure 11. Analysis of proposed four antenna (a) S-parameter (b) realized gain.

Experimental outcomes and diversity parameters

In this section, the experimental outcomes obtained from the antenna prototype are compared with the simulated results. Figure 12 shows the measured and simulated S-parameter of the proposed antenna. It is measured by using Keysight E5071C VNA. After observing Figure 12, it can be said that there is a good correlation between measured and simulated S-parameters. The proposed antenna works in between 2.35 and 2.57 GHz with an isolation level of more than 25 dB. Figure 13 shows the gain (measured and simulated) and radiation efficiency (simulated) for the proposed antenna. Gain is measured by using two antenna methods. It is measured by using one port, while the other port is terminated with a match load. From Figure 13, it is observed that the value of gain is around 5.0 dBi within the operating band, while it is less than -15 dBi outside the operating band. The same pattern is observed with radiation efficiency, i.e. more than 90% outside the operating band, while less than 60% outside the working band. Figure 14 shows the measured and simulated 2D radiation pattern at 2.4 GHz in the XZ and YZ planes. From Figure 14, it is observed that there is more than a 20-dB difference between co-pol and cross-pol radiation pattern. Broadsided radiation pattern confirms the creation of fundamental hybrid mode inside the cylindrical ceramic.

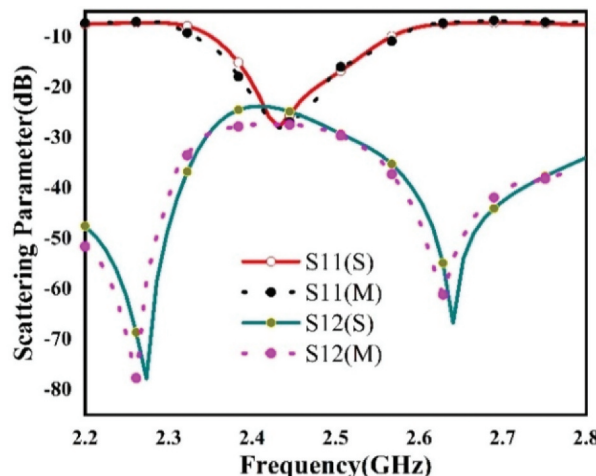


Figure 12. Measured and simulated S-parameter for proposed MIMO radiator.

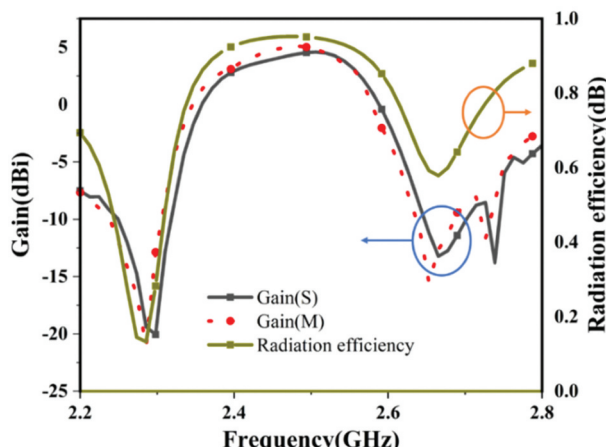


Figure 13. Gain (measured and simulated) and radiation efficiency (simulated) curve for proposed MIMO radiator.

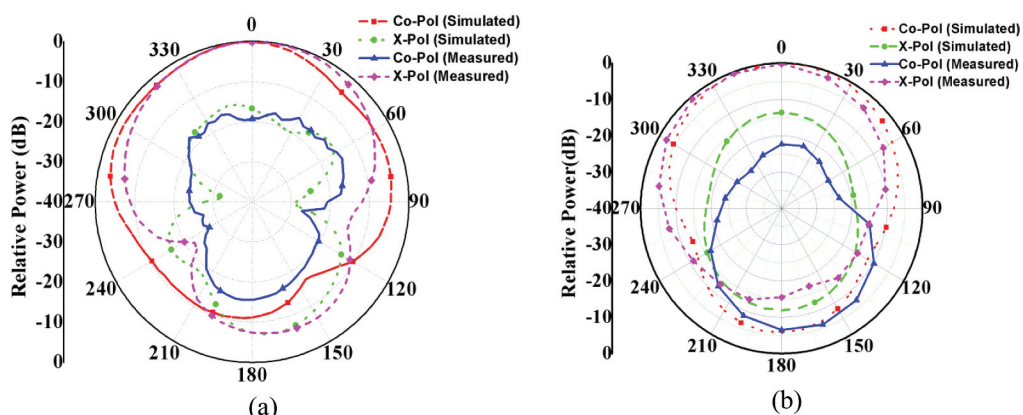


Figure 14. Two-dimensional measured and simulated radiation pattern at 2.4 GHz (a) XZ plane (b) YZ plane.

To mitigate the effects of destructive interference arising from multipath fading, it becomes crucial to implement a suitable antenna diversity scheme. The effectiveness of the suggested filtering MIMO DRA can be assessed using three fundamental performance indicators: the envelope correlation coefficient (ECC), diversity gain (DG), and channel capacity loss (CCL), as elaborated in references (Blanch, Romeu, and Corbella 2003)- (Chae, Oh, and Park 2007). The evaluation of MIMO DRAs' performance entails the utilization of the envelope correlation coefficient (ECC), a metric employed to gauge the likeness of radiation patterns between a pair of antennas. In an ideal scenario where the envelope correlation coefficient (ECC) equals 0, indicating no overlap, the radiation patterns of the two antennas remain distinct. Consequently, incoming signals are captured by individual array elements, irrespective of their direction. Conversely, when the envelope correlation coefficient (ECC) is equal to 1, it signifies that the radiation patterns of the two antennas are identical. This results in an undesirable scenario where the incoming signal is evenly received by both ports. Opting for lower values of the envelope correlation coefficient (ECC) is generally favored, with values below 0.5 being deemed acceptable. The ECC can be computed as follows (Blanch, Romeu, and Corbella 2003):

$$ECC = \left\{ \frac{|S_{11}^* S_{12} + S_{21}^* S_{22}|^2}{[1 - |S_{11}|^2 - |S_{21}|^2][1 - |S_{22}|^2 - |S_{12}|^2]} \right\} \quad (2)$$

Diversity gain (DG) stands as another pivotal parameter utilized to validate the efficacy of MIMO antennas. The approximate correlation between the envelope correlation coefficient (ECC) and diversity gain (DG) is expounded in reference (Rosengren and Kildal 2005). An optimal diversity gain (DG) value of 10 is regarded as ideal, although values exceeding 6 are still considered to fall within an acceptable range, as indicated in reference (Iqbal et al. 2018).

$$DG = 10 * [1 - |ECC|^2]^{0.5} \quad (3)$$

Channel capacity loss (CCL) is intricately influenced by the intricate interplay among multiple antennas, with CCL exhibiting a direct correlation to the number of antenna elements. The augmentation in CCL occurs in tandem with the escalation in the count of these elements. Since the degree of correlation amid the array constituents within a Multiple-Input Multiple-Output (MIMO) channel contributes to CCL, its quantification can be derived through the subsequent calculation (Chae, Oh, and Park 2007).

$$CCL = -\log_2 \det[\psi^R] \quad (4)$$

$$\psi^R = \begin{pmatrix} \rho_{11} & \rho_{12} \\ \rho_{21} & \rho_{22} \end{pmatrix} \quad (5)$$

$$\rho_{jj} = 1 - \{|S_{jj}|^2 + |S_{jk}|^2\} \quad (6)$$

$$\rho_{jk} = -\{S_{jj}^* * S_{jk} + S_{kj}^* * S_{kk}\} \quad (7)$$

Figure 15 shows the measured and simulated ECC and DG for the proposed radiator. From Figure 15, it is observed that the value of ECC is well below 0.01, while the value of DG is

around 10.0 dB for the proposed antenna within the working frequency range. [Figure 16](#) shows the channel capacity loss variation of the proposed antenna. From [Figure 16](#), it can be seen that the value of CCL is well below 4.0 bits/sec/Hz within the working frequency range. [Table 2](#) compares the performance of the proposed DR-based MIMO filtenna with other existing DR-based filtennas. From [Table 2](#), it can be observed that the overall performance of the designed filtenna is better as compared to other existing filtering radiators. The overall size of the four-port MIMO antenna is comparably less as compared to the existing single-port radiator.

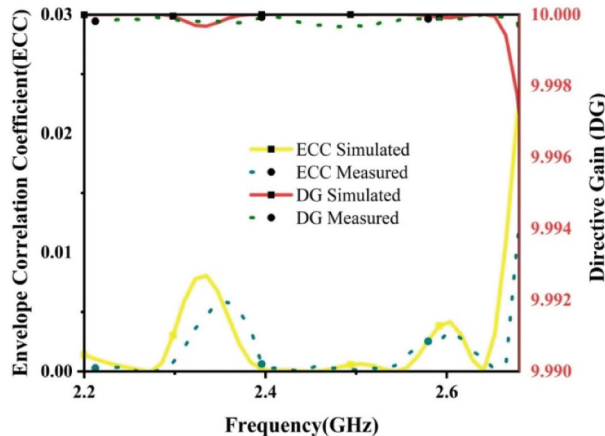


Figure 15. Simulated and measured variation of ECC and DG for proposed antenna.

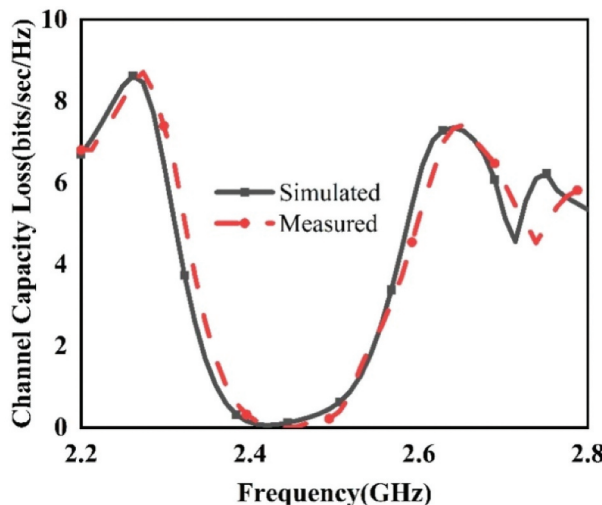


Figure 16. Simulated and measured variation of CCL for the proposed antenna.

Table 2. Performance comparison of proposed MIMO filtenna with other existing DR-based filtenna.

Antenna Design	No. of Antenna ports	Impedance Bandwidth	Gain	Antenna Size (mm ²)
Rectangular DRA (Hu et al. 2016)	01	1.0 GHz	4.0 dBi (within working band) and -20 dBi (outside the working band)	60*43
Rectangular DRA (Hu et al. 2017)	01	2.1 GHz	7.1 dBi (within working band) and -15 dBi (outside the working band)	70*70
Rectangular DRA (Pan et al. 2018)	01	.35 GHz	5.0 dBi (within working band) and -15 dBi (outside the working band)	70*70
Cylindrical DRA (Yadav, Tiwari, and Sharma 2023)	01	.32 GHz	4.5 dBi (within working band) and -12 dBi (outside the working band)	40*40
Rectangular DRA (Liu, Leung, and Yang 2021)	01	.21 GHz	5.0 dBi (within working band) and -15 dBi (outside the working band)	70*53
Rectangular DRA (Wang et al. 2021)	01	.2 GHz	5.1 dBi (within working band) and -15 dBi (outside the working band)	70*70
Proposed DRA	04	.22 GHz	5.0 dBi (within working band) and -15 dBi (outside the working band)	100*100

Conclusion

In this article, four-port dielectric resonator-based filtenna is discussed and analyzed. With the help of the designed feeding mechanism, HEM₁₁₈ mode is stimulated inside the ceramic and makes the proposed radiator employable between 2.35 and 2.57 GHz. Due to the addition of the concept of polarization diversity and space diversity, the value of isolation among the ports is more than 25 dB. The driven rectangular strip and parasitic rectangular strip independently control upper and lower radiation nulls at 2.28 GHz and 2.68 GHz, respectively. This helps to reduce the gain drastically (i.e. -15 dBi) outside the operating band. The stable gain value within the operating band (5.0 dBi) makes the radiator applicable for IoT applications.

Disclosure statement

No potential conflict of interest was reported by the author(s).

ORCID

Anand Sharma  <http://orcid.org/0000-0001-8566-1710>

References

- Blanch, S., J. Romeu, and I. Corbella. 2003, May. Exact representation of antenna system diversity performance from input parameter description. *Electronics Letters* 39 (9):705–707. doi:[10.1049/el:20030495](https://doi.org/10.1049/el:20030495).
- Chae, S. H., S. K. Oh, and S.-O. Park. 2007. Analysis of mutual coupling, correlations, and TARC in WiBro MIMO array antenna. *IEEE Antennas & Wireless Propagation Letters* 6:122–25. doi:[10.1109/LAWP.2007.893109](https://doi.org/10.1109/LAWP.2007.893109).
- Dhwaj, K., J. M. Kovitz, H. Z. Tian, L. J. Jiang, and T. Itoh. 2018. Half-mode cavity based planar filtering antenna with controllable transmission zeroes. *IEEE Antennas & Wireless Propagation Letters* 17 (5):833. doi:[10.1109/LAWP.2018.2818058](https://doi.org/10.1109/LAWP.2018.2818058).
- Hu, P. F., Y. M. Pan, K. W. Leung, and X. Y. Zhang. 2018, May. Wide-/dual-band omnidirectional filtering dielectric resonator antennas. *IEEE Transactions on Antennas & Propagation* 66 (5):2622–27. doi:[10.1109/TAP.2018.2809706](https://doi.org/10.1109/TAP.2018.2809706).
- Hu, P. F., Y. M. Pan, X. Y. Zhang, and S. Y. Zheng. 2016, Aug. A compact filtering dielectric resonator antenna with wide bandwidth and high gain. *IEEE Transactions on Antennas & Propagation* 64 (8):3645–51. doi:[10.1109/TAP.2016.2565733](https://doi.org/10.1109/TAP.2016.2565733).
- Hu, P. F., Y. M. Pan, X. Y. Zhang, and S. Y. Zheng. 2017, Apr. Broadband filtering dielectric resonator antenna with wide stopband. *IEEE Transactions on Antennas & Propagation* 65 (4):2079–84. doi:[10.1109/TAP.2017.2670438](https://doi.org/10.1109/TAP.2017.2670438).
- Iqbal, A., O. A. Saraereh, A. W. Ahmad, and S. Bashir. 2018. Mutual coupling reduction using F-shaped stubs in UWB-MIMO antenna. *Institute of Electrical and Electronics Engineers Access* 6:2755–2759. doi:[10.1109/ACCESS.2017.2785232](https://doi.org/10.1109/ACCESS.2017.2785232).
- Jin, J. Y., S. Liao, and Q. Xue. 2018, Apr. Design of filtering-radiating patch antennas with tunable radiation nulls for high selectivity. *IEEE Transactions on Antennas & Propagation* 66 (4):2125–30. doi:[10.1109/TAP.2018.2804661](https://doi.org/10.1109/TAP.2018.2804661).
- Liu, X. Y., K. W. Leung, and N. Yang. 2021, Jun. Frequency reconfigurable filtering dielectric resonator antenna with harmonics suppression. *IEEE Transactions on Antennas & Propagation* 69 (6):3224–33. doi:[10.1109/TAP.2020.3044387](https://doi.org/10.1109/TAP.2020.3044387).

- Mao, C. X., S. Gao, Y. Wang, B. Sanz-Izquierdo, Z. Wang, F. Qin, Q. X. Chu, J. Li, G. Wei, and J. Xu. **2016**, Sep. Dual-band patch antenna with filtering performance and harmonic suppression. *IEEE Transactions on Antennas & Propagation* 64 (9):4074–77. doi:[10.1109/TAP.2016.2574883](https://doi.org/10.1109/TAP.2016.2574883).
- Martin, J., Y. Antar, A. Kishk, A. Ittipiboon, and M. Cuhaci. , Dielectric resonator antenna using aperture coupling. *Electronics Letters* 26 (24):2015–16. doi:[10.1049/el:19901302](https://doi.org/10.1049/el:19901302).
- Pan, Y. M., P. F. Hu, K. W. Leung, and X. Y. Zhang. **2018**, Sep. Compact single-/dual-polarized filtering dielectric resonator antennas. *IEEE Transactions on Antennas & Propagation* 66 (9):4474–84. doi:[10.1109/TAP.2018.2845457](https://doi.org/10.1109/TAP.2018.2845457).
- Petosa, A. **2007**. *Dielectric resonator antenna handbook*. Norwood, MA, USA: Artech House.
- Rosengren, K., and P.-S. Kildal. **2005**. Radiation efficiency, correlation, diversity gain and capacity of a six-monopole antenna array for a MIMO system: Theory, simulation and measurement in reverberation chamber. *IEE Proceedings - Microwaves, Antennas and Propagation* 152 (1):7–16. doi:[10.1049/ip-map:20045031](https://doi.org/10.1049/ip-map:20045031).
- Sharawi, M. S. **2014**. *Printed MIMO antenna engineering*. Boston, London: Artech House.
- Wang, C. Y., Z. W. Han, H. W. Liu, P. Wen, L. N. Wang, and X. Q. Zhang. **2021**, Nov. A novel single-feed filtering dielectric resonator antenna using slot line stepped-impedance resonator. *IEEE Transactions on Circuits & Systems II: Express Briefs* 68 (11):3426–30. doi:[10.1109/TCSII.2021.3079636](https://doi.org/10.1109/TCSII.2021.3079636).
- Yadav, A., M. Tiwari, and A. Sharma. **2023**, Feb. Dual-band quasi-isotropic dielectric resonator-based filtering antenna for IoT applications. *Journal of Electronic Materials* 52 (2):1590–8. doi:[10.1007/s11664-022-10133-8](https://doi.org/10.1007/s11664-022-10133-8).
- Yusuf, Y., H. Cheng, and X. Gong. **2011**, Nov. A seamless integration of 3-D vertical filters with highly efficient slot antennas. *IEEE Transactions on Antennas & Propagation* 59 (11):4016–22. doi:[10.1109/TAP.2011.2164186](https://doi.org/10.1109/TAP.2011.2164186).